ACS APPLIED MATERIALS & INTERFACES

Research Article

www.acsami.org

Polymer/Graphene Hybrid Aerogel with High Compressibility, Conductivity, and "Sticky" Superhydrophobicity

Han Hu,[†] Zongbin Zhao,*[,†] Wubo Wan,[†] Yury Gogotsi,[†,‡] and Jieshan Qiu*[,†]

[†]Carbon Research Laboratory, Liaoning Key Lab for Energy Materials and Chemical Engineering, State Key Lab of Fine Chemicals, School of Chemical Engineering, Dalian University of Technology, Dalian 116023, People's Republic of China

[‡]Department of Materials Science and Engineering and A.J. Drexel Nanotechnology Institute, Drexel University, Philadelphia, Pennsylvania 19104, United States

Supporting Information

ABSTRACT: The idea of extending functions of graphene aerogels and achieving specific applications has aroused wide attention recently. A solution to this challenge is the formation of a hybrid structure where the graphene aerogels are decorated with other functional nanostructures. An infiltration−evaporation−curing strategy has been proposed by the formation of hybrid structure containing poly(dimethylsiloxane) (PDMS) and compressible graphene aerogel (CGA), where the cellular walls of the CGA are coated uniformly with an integrated polymer layer. The resulting composite shows enhanced compressive strength and a stable Young's modulus that are superior to those of pure CGAs. This unique structure combines the advantages of both components, giving rise to an excellent electromechanical performance, where the bulk resistance repeatedly shows a synchronous and linear response to variation of the volume during compression at a wide range of compressed rates. Furthermore, the foamlike structure delivers a water droplet with "sticky" superhydrophobicity and a size as large as 32 μL that remains tightly pinned to the composite, even when it is turned upside-down. This is the first demonstration of superhydrophobicity with strong adhesion on a foamlike structure. These outstanding properties qualify the PDMS/CGA composites developed here as promising candidates for a wide range of applications such as in sensors, actuators, and materials used for biochemical separation and tissue engineering.

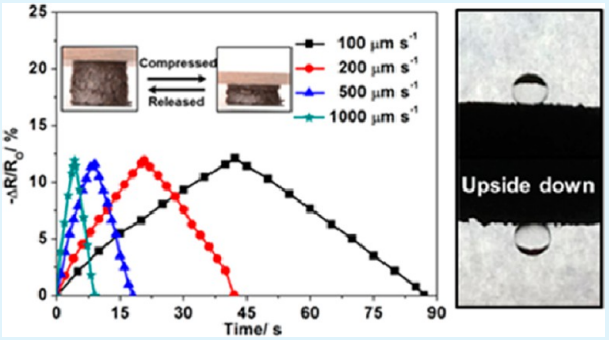

KEYWORDS: *graphene aerogel, compressibility, poly(dimethylsiloxane), electromechanical performance, synergistic effect, superhydrophobicity*

INTRODUCTION

Carbon aerogels represent an attractive form of carbon monoliths with practical importance because of their light weight, high porosity, large surface area, and electrical conductivity.[1−3] These structures can be easily produced by carbonization of polymer aerogels produced using sol−gel chemistry[1,4] and the assembly of novel carbon nanomaterials such as carbon nanotubes,[5−10] carbon nanofibers,[11] graphene,[12−20] and their composites.[21−29] Recently, the boom of graphene has aroused wide attention to graphene aerogels, which can harvest the attractive properties of graphene for macroscopic applications.[30] As such, a series of methods have been established to produce graphene aerogels, including hydrothermal reduction,[13,16,18] chemical reduction,[15,19,20] and template-directed chemical vapor deposition.[30,31] Chemically converted graphene nanosheets have been widely utilized as building blocks for the integration of aerogel-like materials due to the diversity in controlling the structures and properties during assembly.[12−20] However, the idea of extending functions of graphene aerogels and achieving specific applications is also highly demanded and requires the formation of hybrid strucutres.[24,25,30,31] Using a functionalization−lyophilization−microwave treatment approach,[15] we reported a compressible graphene aerogel (CGA) with a porosity of up to 99.8% and excellent compressibility. The CGA consists of wrinkled cell walls with an in-plane size of tens to hundreds of microns. These features may allow CGA to be a promising candidate for formation of a hybrid strucutre with outstanding properties such as attractive wettability when combined with materials of low surface energy.

Herein, we present an infiltration−evaporation−curing strategy for the fabrication of a poly(dimethylsiloxane) (PDMS)/CGA hybrid structure, where an integrated PDMS layer is formed on the cellular walls of a CGA scaffold, leading to a greatly improved mechanical performance. Furthermore, the unique monolithic structure consisting of graphene@PDMS demonstrates an excellent electromechanical performance required in electrical devices such as sensors and actuators.

Received: November 11, 2013
Accepted: February 13, 2014
Published: February 13, 2014

   dx.doi.org/10.1021/am4050647 | ACS Appl. Mater. Interfaces 2014, 6, 3242−3249

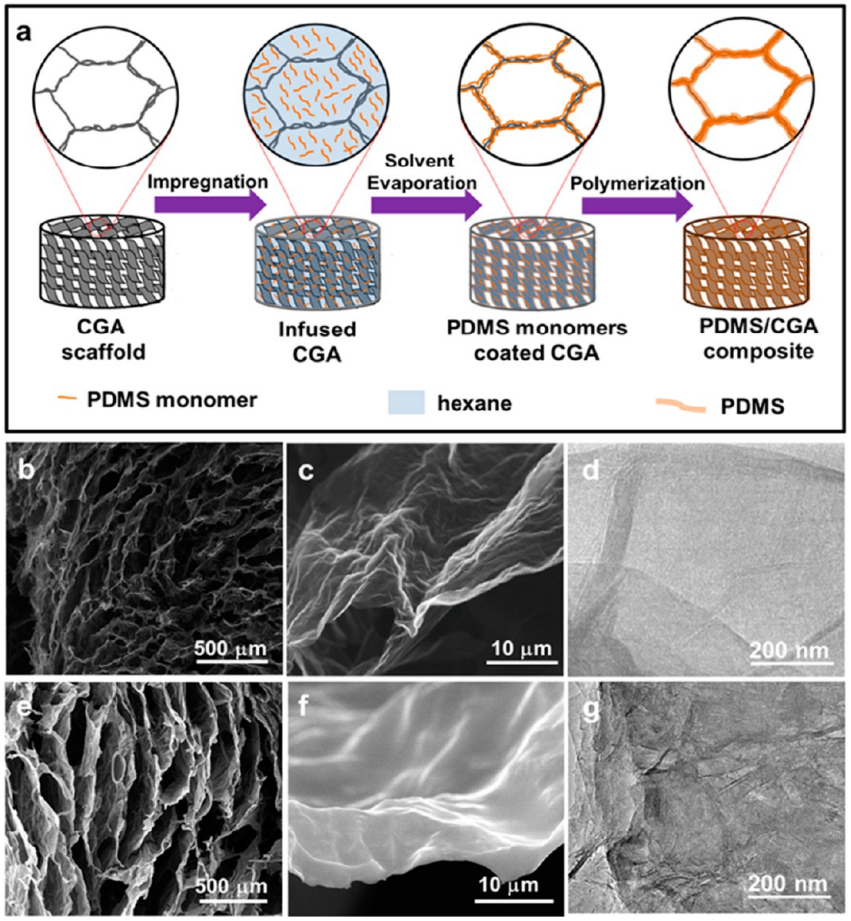

Figure 1. (a) Schematic illustration of the fabrication process of PDMS/CGA. SEM images of the porous structure (b) and cellular wall (c) of the CGA. (d) TEM image of the CGA. SEM images of the porous structure (e) and cellular wall (f) of PDMS/CGA. (g) TEM image of PDMS/CGA.

Also, spherical water droplets remain pinned to PDMS/CGA without falling off, even after being turned upside-down. This is the first time that this "sticky" superhydrophobicity has been observed for a foamlike structure, leading to potential applications in biochemical separation, microdroplet transport, tissue engineering, and microfluidic chips.

EXPERIMENTAL SECTION

Synthesis of a Compressible Graphene Aerogel (CGA). CGAs were synthesized via a functionalization−lyophilization−microwave treatment process reported elsewhere.[15] In a typical synthesis process, a graphene oxide (GO) dispersion (3 mg mL^{-1}, 5 mL) was mixed with ethylenediamine (20 μL) in a glass vial with an inner diameter of 20 mm before reaction at 95 °C for 6 h. After formation of a functionalized graphene hydrogel, a freeze-drying process was used to remove the solvent within the gel. Then, the as-obtained functionalized graphene aerogel was exposed to microwave irradiation for 1 min in an argon atmosphere, giving rise to the CGA.

Fabrication of Poly(dimethylsiloxane) (PDMS)/CGA. The as-prepared CGA was first immersed into a hexane solution of the PDMS monomer and a curing agent. The mass ratio of hexane, PDMS monomer, and curing agent was set in a wide range from 9000:10:1 to 4:10:1. The mixture of PDMS and curing agent without hexane was also used to infiltrate the pores of CGAs. Then, the infused CGAs were transferred into a vacuum oven and heated to 120 °C to remove the solvent, thus allowing the PDMS monomer and curing agent to be concentrated on the surface of the cellular wall. Afterward, the structure was further heated at 120 °C to induce the polymerization reaction, resulting in the production of PDMS/CGA.

Fabrication of a Pure PDMS Film. A pure PDMS film was synthesized by first uniformly mixing the PDMS monomer and curing agent with a mass ratio of 10:1. Then, the mixture was coated on a glass plate and heated at 120 °C overnight under a vacuum to remove gas bubbles and induce polymerization.

Characterization of the Composite. The porous structure of the composite was observed on a QUANTA 450 scanning electron microscope, while an FEI TF30 transmission electron microscope recorded the detailed morphologies of the cellular walls. Raman spectra of PDMS, CGA, and PDMS/CGA were performed on a DXR Raman microscope (Thermo Scientific) with an excitation wavelength of 532 nm. The compressibility was tested via a method reported elsewhere.[15,32,33] This process typically involves loading a monolith between a compressible head and pressure sensor, where the displacement and corresponding stress values were recorded. All of the stress−strain curve measurements were conducted at a compression speed of 1 mm s^{-1}. In order to test the electromechanical performance, the monolith was glued between two plates using a silver paste, where metal wires were connected to an electrochemical workstation (CHI 760D) to record variation of either the current or voltage. The $I-V$ curves were obtained via linear sweep voltammetry. The voltage range was typically set between −0.2 and +0.2 V. Variation of the bulk resistance with strain was conducted by generating an amperometric $i-t$ curve. In this process, the voltage was fixed at 0.1 V and variation of the current was recorded as a function of time, allowing for the resistance to be obtained by dividing the current at each time point by the voltage. The water contact angles (WCAs) were measured by the goniometry method, where images of droplets with 4 μL of water resting on the monolith surfaces were captured, and the WCAs were determined using *JC2000C1* software

dx.doi.org/10.1021/am4050647 | *ACS Appl. Mater. Interfaces* 2014, 6, 3242−3249

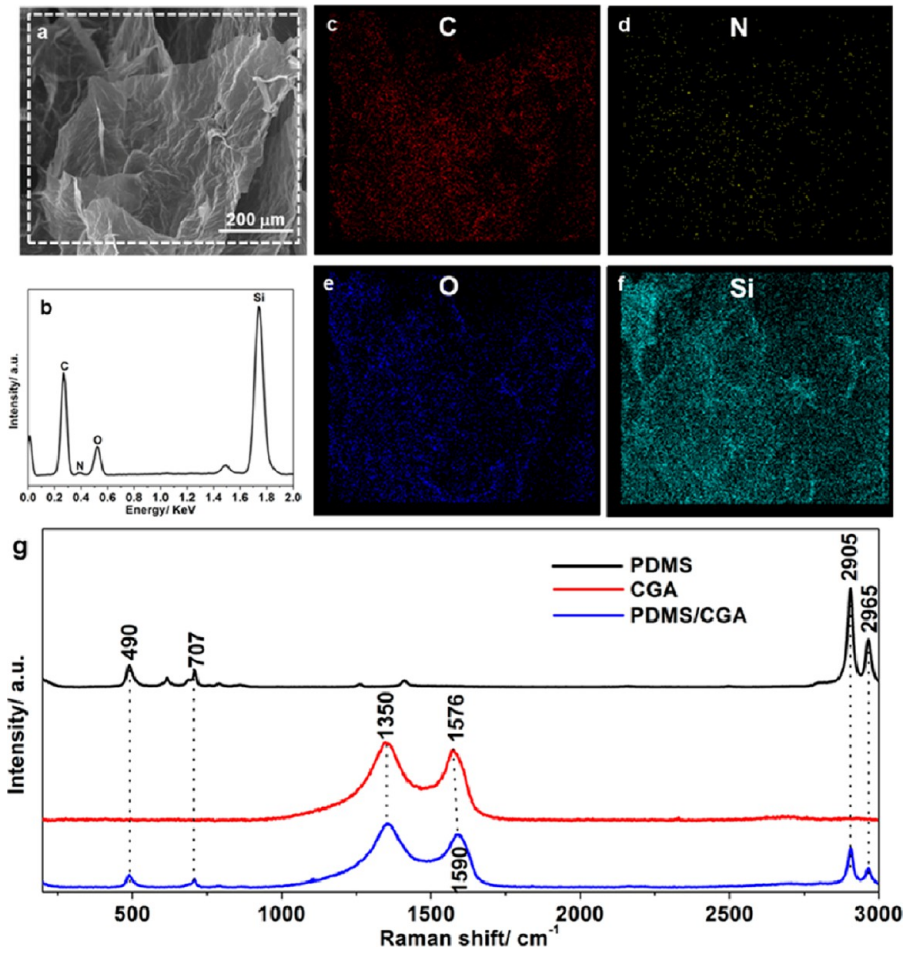

Figure 2. Elemental maps and Raman spectra. (a) SEM image of PDMS/CGA. (b) EDX spectrum and (c) carbon, (d) nitrogen, (e) oxygen, and (f) silicon maps of PDMS/CGA taken in the rectangular area in part a. (g) Raman spectra of PDMS, CGA, and PDMS/CGA.

(Powereach, China). The structure analysis and property testing were conducted on PDMS/CGA with a graphene content of about 17 wt %.

RESULTS AND DISCUSSION

The fabrication process of PDMS/CGA includes three main steps, as illustrated in Figure 1a. First, the as-prepared CGA[15] was immersed in a hexane solution containing the PDMS monomer and curing agent, with a mass ratio of 10:1. The strong affinity of graphene for the organic solvent[16,17,26,31] allows for full infiltration of the solution into the CGA pores. Then, the infused CGA was transferred into a vacuum oven and heated to 120 °C to remove hexane, causing the PDMS monomer and curing agent to congregate on the cellular walls of the CGA. After that, the material was further heated at 120 °C overnight to induce polymerization of PDMS on the cellular walls of the CGA, giving rise to the fully formed PDMS/CGA composite.

Digital images of PDMS/CGAs are shown in Figure S1 in the Supporting Information (SI). The composites can be easily crafted into different morphologies such as rods, cylinders, and cuboids (Figure S1 in the SI) because of the convenient formation of graphene aerogels with various shapes.[18,19] Furthermore, the PDMS/CGAs can be easily manufactured on a large scale by carrying out the synthesis process on CGAs with larger sizes, exhibited in Figure S1 in the SI. The microscopic observation reveals that CGAs have a foamlike structure containing interconnected pores in the range of tens to hundreds of microns (Figure 1b) and highly wrinkled cell wall surfaces (Figure 1c,d). As shown in Figure 1e, PDMS/CGA exhibits a foamlike structure similar to that of pure CGA, indicating that PDMS is mainly distributed on the cell wall surfaces instead of filling the pores. The direct observation of cell walls (Figure 1f,g) reveals increased thickness because the sheets are less transparent under an electron beam, thus confirming the successful coating of the cellular walls with the polymer layer. The wrinkles and folds of the CGA after coating with PDMS are partially maintained; concaves of several microns and folds of hundreds of nanometers can be observed (Figures 1f and in the SI).

The material composition and elemental distributions of PDMS/CGA are both illustrated in Figure 2. The energy dispersive X-ray (EDX) spectrum (Figure 2b) taken in the rectangular region of Figure 2a mainly contains four elements, including carbon, nitrogen, oxygen, and silicon, all of which are distributed homogenously (Figure 2c–f), thus indicating the uniform distribution of PDMS on the CGA's wall surfaces. This result is in good agreement with SEM (Figure 1e,f) and TEM (Figure 1g) observations. The Raman spectra of PDMS, CGA, and PDMS/CGA are compared in Figure 2g. The pure PDMS mainly exhibits four peaks at 2965, 2905, 707, and 490 cm^{-1} associated with the asymmetric and symmetric vibrations of CH_3, the symmetric stretching of Si–C, and the symmetric stretching of Si–O–Si,[34] while the CGA shows two dominant peaks at 1350 and 1576 cm^{-1}, corresponding to the D and G

dx.doi.org/10.1021/am4050647 | ACS Appl. Mater. Interfaces 2014, 6, 3242–3249

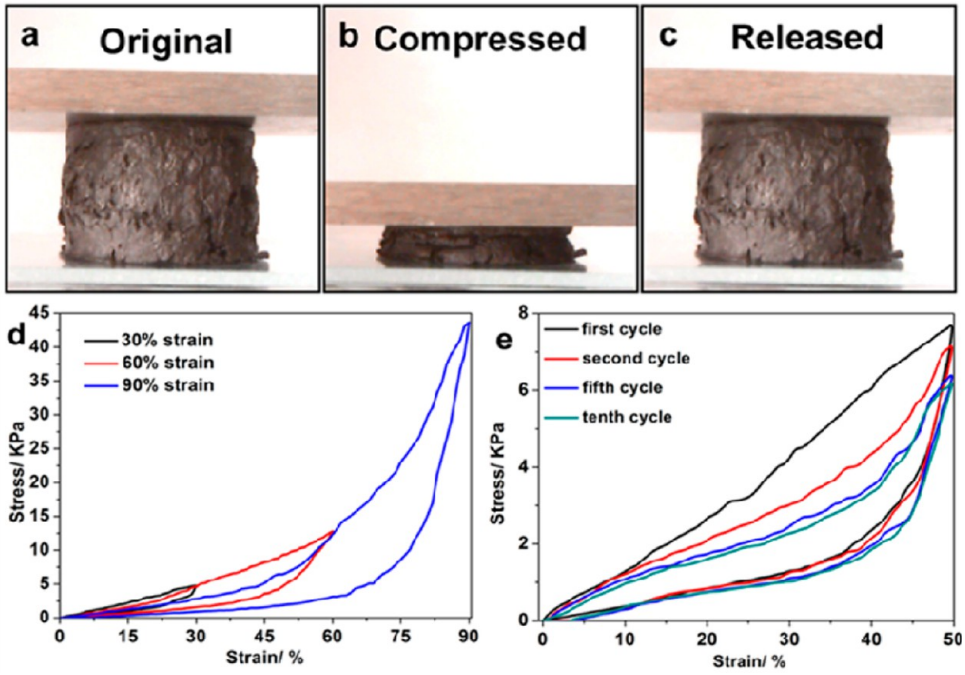

Figure 3. Compressibility of PDMS/CGA. (a–c) Digital images of a typical compression process of PDMS/CGA. Stress–strain curves of PDMS/CGA at different maximum strains (d) and at a strain of 50% for 10 cycles (e).

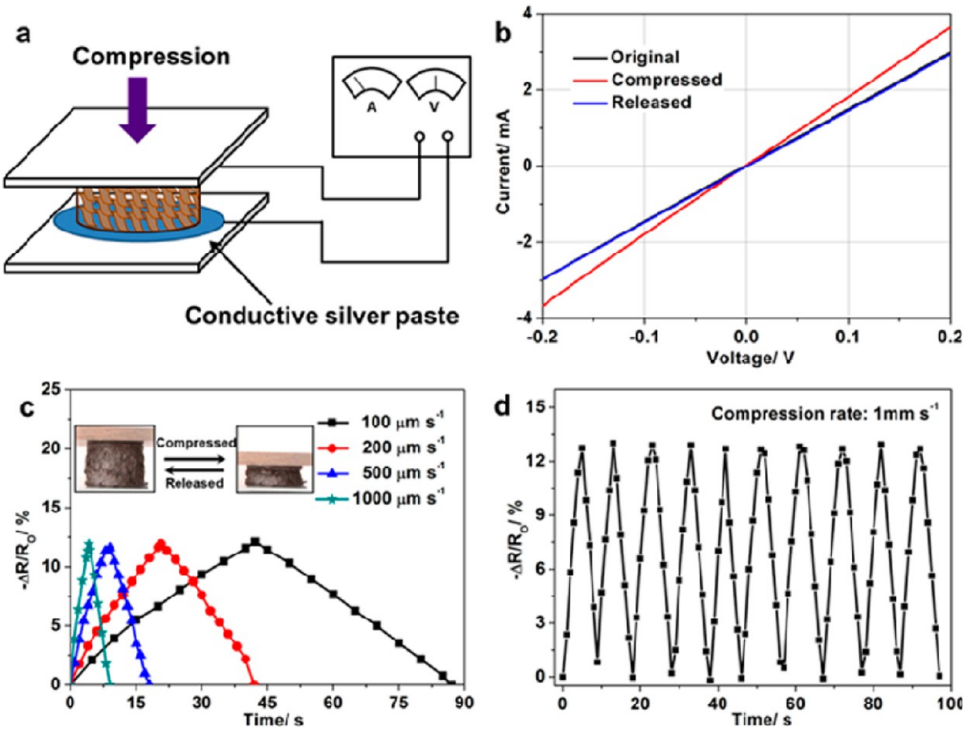

Figure 4. Electromechanical performance of PDMS/CGA. (a) Illustration of the test setup for the electromechanical properties. (b) *I*–*V* curves of the original, compressed, and released PDMS/CGA. (c) Variation of the resistance of PDMS/CGA with strain up to 50% at different compression rates. (d) Variation of the resistance of the composite with strain up to 50% at a compression rate of 1 mm s^{-1} for multicycles.

bands of graphitic carbon (Table S1 in the SI).[35] The PDMS/CGA composite exhibits all of the bands of both PDMS and CGA at the same position, except the red shift of the G band from 1576 cm^{-1} for CGA to 1590 cm^{-1} for PDMS/CGA. When bonds form between carbon and other components, charge transfer between them could result in the red shift of the G band of carbon.[36−39] Thus, a 14 cm^{-1} shift in the G band may indicate the formation of bonds between PDMS and chemically converted graphene.

The compression tests of PDMS/CGA are shown in Figure 3. The monolith is able to be squeezed into a small pellet under pressure, resulting in up to 90% strain, and recovers immediately after the external force has been removed (Figure 3a). It should be noted that cracks may form on the outer

dx.doi.org/10.1021/am4050647 | ACS Appl. Mater. Interfaces 2014, 6, 3242−3249

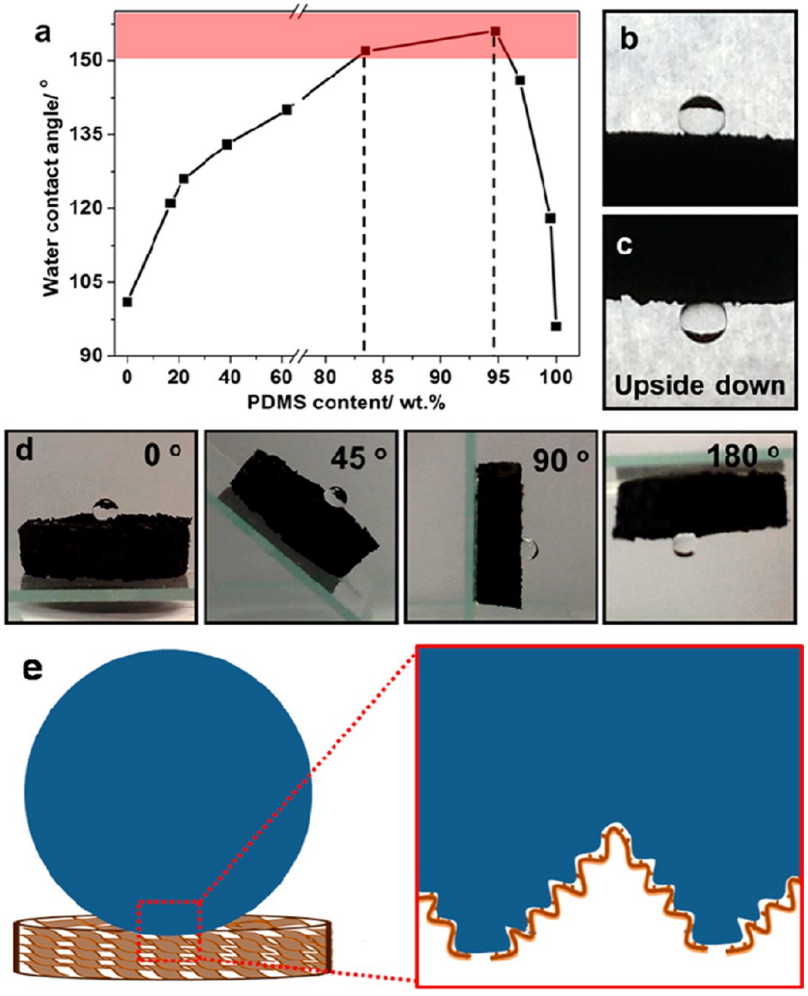

Figure 5. Wettability of PDMS/CGA. (a) Variation of the WCAs with the PDMS content. (b) Shape of the water droplet on PDMS/CGA (PDMS, 83 wt %) (c) Shape of the water droplet on PDMS/CGA (PDMS, 83 wt %) when turned upside-down. (d) Water droplet on a rotated composite. (e) Schematic illustration of a water drop in contact with the foam.

surface of pure CGAs after this type of extreme compression is applied.[15,24] However, the exterior of PDMS/CGA remains the same, without the formation of any cracks. Even after repeated compressions at a wide range of speeds, from 1 to 5 mm s^{-1}, the volume and outer surface remain unchanged without any discernible deformation (Figures S3 and S4 and Movie S1 in the SI). The stress−strain curves of PDMS/CGA at 30%, 60%, and 90% strain are shown in Figure 3c. The linear-elastic region of PDMS/CGA can be extended up to a 60% strain, much higher than that of pure CGAs and other carbon aerogels.[11,12,15,22] The densification region appears at strains larger than 60%, where the stress increases dramatically and the maximum compressive stress at 90% strain approaches 43 kPa. As reported previously, the corresponding value for CGAs is only around 20 kPa (Figure S5a in the SI).[12,15] The increased compressive stress may associate with chemical bonding of the polymer on the outmost layers of cellular walls. The mechanical performance may be further improved by intercalating polymer between graphene layers due to more chemical bonds.[25] After unloading, the formed hysteresis loops indicate an elastic foam structure.[11,22,40] The cyclic compression test, with 50% strain, is shown in Figure 3d. The curve for the first cycle remains linear for almost the entire loading process. However, after this first loading, the curves for the remaining cycles depart from linearity. After repeated compressions, the Young's modulus of the composite is discerned and compared to the initial value by dividing the Young's modulus in each cycle by that of the first cycle. As shown in Figure S5b and Table S2 in the SI, the Young's modulus for the second cycle decreases to 89% and, finally, to 73% after 10 cycles for PDMS/CGA. However, the Young's modulus remains only at 24% of the maximum value after 10 cycles for pure CGAs. Furthermore, PDMS/CGA also delivers a stable energy loss coefficient over cycles, while the percentage of energy dissipated over cycles decreases more rapidly over repeated compression for CGA. The mechanical performances of several other kinds of carbon aerogels have been compared, and PDMS/CGA shows a wide elastic region and relatively high compressive stress at the same strain (Table S3 in the SI).

The electromechanical performance of the composite was tested in the setup illustrated in Figure 4a. The hybrid monolith was glued between two plates by silver paste, where two metal wires were connected with an electrochemical workstation. As shown in Figure 4b, the $I-V$ curve of the original PDMS/CGA exhibits typical linear ohmic behavior. The compressed monolith (ε = 50%) also exhibits this behavior but instead with an increased slope, reflecting the decreased resistance. On the other hand, the $I-V$ curve of the released hybrid structure coincides with that of the original one, thus demonstrating full restoration of the electrical conductivity after unloading.[41] This

result is in good agreement with the greatly improved compressibility and recovery observed for this material. The resistance of PDMS/CGA changes synchronously with that of the volume during loading and unloading. As shown in Figure 4c, variation of the resistance shows a linear relationship with that of the volume, where the resistance decreases linearly during the loading process (Figure 4b,c) and vice versa. This linear relationship exists regardless of the compression rate, at least within the range of 100−1000 μm s^{-1} (Figure 4c). During repeated compression, the linear relationship between variation of the bulk resistance and the volume is well-maintained, demonstrating high electromechanical stability.

Both CGAs and pure PDMS films show compromised hydrophobicity. As shown in Figure 5a, the WCA for pure CGA is around 100° because of the presence of heteroatoms, such as oxygen and nitrogen, uniformly distributed on the surface.[15] The PDMS film obtained by direct polymerization exhibits a similar WCA associated with near-flatness.[42] The integration of CGA and PDMS gives rise to enhanced hydrophobicity, as reflected by the increased WCAs. When the content of PDMS is around 83−94 wt % in the composite, a superhydrophobic surface is achieved. After a further increase in the PDMS content, the WCAs decrease even more because of blockage of the CGA pores. Surprisingly, the spherical droplet can remain pinned to the superhydrophobic surface without sliding, even when turned upside-down (Figure 5b,c), indicating strong adhesion.[43,44] Snapshots of the water droplet resting on a rotating foam were illustrated (Figure 5d). During the whole rotating process, the droplet remained in the same position without any sliding (Movie S2 in the SI). The strong affinity is further illustrated by the amount of water that could be suspended on the upside-down foam. As shown in Figure S6 in the SI, as much as 32 μL of water can be tightly pinned to the inverse composite. This property is vastly required in a wealth of applications, such as biochemical separation, transport of microdroplets, tissue engineering, and microfluidic chips.[44−48] The water droplets can be expected to partially penetrate into the pores of PDMS/CGA but cannot form direct contact with the cellular surface because of the presence of wrinkles and folds on the surface, leading to the Cassie impregnating wetting regime, as illustrated in Figure 5e.[44,49] Thus, the partially sealed water can be pinned to the surface, similar to that of the rose petal. As such, it can be deduced that cooperation of the hierarchically rough surface of the cell walls of CGAs and the low surface energy of the PDMS films leads to "sticky" superhydrophobicity. To the best of our knowledge, this is the first demonstration of superhydrophobicity with strong adhesion on a foamlike structure, whereas the widely established methods for "sticky" superhydrophobicity are mainly achieved by creating ordered microscopic arrays on filmlike structures involving sophisticated equipments or time-consuming processes.[42,43,48] The strategy developed here has proved to be a time- and cost-effective method to develop a superhydrophobic structure with high adhesion.

CONCLUSIONS

In summary, an infiltration−evaporation−curing method has been proposed to produce a PMDS/CGA composite, where the polymer layers are uniformly coated on the cellular wall of the CGA. The corresponding structure shows greatly enhanced strength in compression and a stable Young's modulus over repeated compression cycles. The composite also demonstrates an excellent electromechanical performance, and variation of the resistance shows a linear relationship with the strain. The PDMS/CGA composite exhibits superhydrophobicity, yet the droplet can be pinned tightly onto the foam without sliding, even after being turned upside-down. This is the first example of a foamlike structure showing "sticky" superhydrophobicity. These properties of PDMS/CGA may be useful for a wide range of potential applications, including sensors, actuators, and materials for biochemical separation and tissue engineering. We believe that the multifunctional monolithic structure developed using this time- and cost-effective method may pave the way for practical applications of graphene.

ASSOCIATED CONTENT

Supporting Information

Movies and images of hybrid aerogels with different sizes, surface and structure analysis, and a comparison of the compressibility of different kinds of aerogels as well as the rotating process. This material is available free of charge via the Internet at http://pubs.acs.org.

AUTHOR INFORMATION

Corresponding Authors

*E-mail: zbzhao@dlut.edu.cn.
*E-mail: jqiu@dlut.edu.cn.

Notes

The authors declare no competing financial interest.

ACKNOWLEDGMENTS

This work was supported by the NSFC (Grants 51072028 and 20836002). Collaboration between Drexel University and Dalian University of Technology was supported by the Cheung Kong Scholarship. The authors are thankful to Amanda Pentecost (Drexel University) for helpful comments on the manuscript.

REFERENCES

(1) Pierre, A. C.; Pajonk, G. M. Chemistry of Aerogels and Their Applications. *Chem. Rev.* **2002**, *102*, 4243−4265.
(2) Feng, J. Z.; Zhang, C. R.; Feng, J.; Jiang, Y. G.; Zhao, N. Carbon Aerogel Composites Prepared by Ambient Drying and Using Oxidized Polyacrylonitrile Fibers as Reinforcements. *ACS Appl. Mater. Interfaces* **2011**, *3*, 4796−4803.
(3) Wang, Y. J.; Zhao, G. H.; Chai, S. N.; Zhao, H. Y.; Wang, Y. B. Three-Dimensional Homogeneous Ferrite−Carbon Aerogel: One Pot Fabrication and Enhanced Electro-Fenton Reactivity. *ACS Appl. Mater. Interfaces* **2013**, *5*, 842−852.
(4) Pekala, R. W.; Alviso, C. T.; Lemay, J. D. Organic Aerogels—Microstructural Dependence of Mechanical-Properties in Compression. *J. Non-Cryst. Solids* **1990**, *125*, 67−75.
(5) Pathak, S.; Cambaz, Z. G.; Kalidindi, S. R.; Swadener, J. G.; Gogotsi, Y. Viscoelasticity and High Buckling Stress of Dense Carbon Nanotube Brushes. *Carbon* **2009**, *47*, 1969−1976.
(6) Gogotsi, Y. High-Temperature Rubber Made from Carbon Nanotubes. *Science* **2010**, *330*, 1332−1333.
(7) Gui, X.; Wei, J.; Wang, K.; Cao, A.; Zhu, H.; Jia, Y.; Shu, Q.; Wu, D. Carbon Nanotube Sponges. *Adv. Mater.* **2010**, *22*, 617−621.
(8) Cao, A.; Dickrell, P. L.; Sawyer, W. G.; Ghasemi-Nejhad, M. N.; Ajayan, P. M. Super-Compressible Foam Like Carbon Nanotube Films. *Science* **2005**, *310*, 1307−1310.
(9) Xu, M.; Futaba, D. N.; Yamada, T.; Yumura, M.; Hata, K. Carbon Nanotubes with Temperature-Invariant Viscoelasticity from −196 degrees to 1000 degrees C. *Science* **2010**, *330*, 1364−1368.
(10) Pathak, S.; Lim, E. J.; Pour Shahid Saeed Abadi, P.; Graham, S.; Cola, B. A.; Greer, J. R. Higher Recovery and Better Energy

Dissipation at Faster Strain Rates in Carbon Nanotube Bundles: An in-Situ Study. *ACS Nano* **2012**, *6*, 2189−2197.
(11) Liang, H. W.; Guan, Q. F.; Chen, L. F.; Zhu, Z.; Zhang, W. J.; Yu, S. H. Macroscopic-Scale Template Synthesis of Robust Carbonaceous Nanofiber Hydrogels and Aerogels and Their Applications. *Angew. Chem., Int. Ed.* **2012**, *51*, 5191−5195.
(12) Qiu, L.; Liu, J. Z.; Chang, S. L. Y.; Wu, Y. Z.; Li, D. Biomimetic Superelastic Graphene-Based Cellular Monoliths. *Nat. Commun.* **2012**, *3*, 1241.
(13) Xu, Y. X.; Sheng, K. X.; Li, C.; Shi, G. Q. Self-Assembled Graphene Hydrogel via a One-Step Hydrothermal Process. *ACS Nano* **2010**, *4*, 4324−4330.
(14) Worsley, M. A.; Kucheyev, S. O.; Mason, H. E.; Merrill, M. D.; Mayer, B. P.; Lewicki, J.; Valdez, C. A.; Suss, M. E.; Stadermann, M.; Pauzauskie, P. J.; Satcher, J. H.; Biener, J.; Baumann, T. F. Mechanically Robust 3D Graphene Macroassembly with High Surface Area. *Chem. Commun.* **2012**, *48*, 8428−8430.
(15) Hu, H.; Zhao, Z. B.; Wan, W. B.; Gogotsi, Y.; Qiu, J. S. Ultralight and Highly Compressible Graphene Aerogels. *Adv. Mater.* **2013**, *25*, 2219−2223.
(16) Bi, H. C.; Xie, X.; Yin, K. B.; Zhou, Y. L.; Wan, S.; He, L. B.; Xu, F.; Banhart, F.; Sun, L. T.; Ruoff, R. S. Spongy Graphene as a Highly Efficient and Recyclable Sorbent for Oils and Organic Solvents. *Adv. Funct. Mater.* **2012**, *22*, 4421−4425.
(17) Zhao, Y.; Hu, C. G.; Hu, Y.; Cheng, H. H.; Shi, G. Q.; Qu, L. T. A Versatile, Ultralight, Nitrogen-Doped Graphene Framework. *Angew. Chem., Int. Ed.* **2012**, *51*, 11371−11375.
(18) Bi, H. C.; Yin, K. B.; Xie, X.; Zhou, Y. L.; Wan, N.; Xu, F.; Banhart, F.; Sun, L. T.; Ruoff, R. S. Low Temperature Casting of Graphene with High Compressive Strength. *Adv. Mater.* **2012**, *24*, 5124−5129.
(19) Yan, L. F.; Chen, W. F. In Situ Self-Assembly of Mild Chemical Reduction Graphene for Three-Dimensional Architectures. *Nanoscale* **2011**, *3*, 3132−3137.
(20) Zhang, X. T.; Sui, Z. Y.; Xu, B.; Yue, S. F.; Luo, Y. J.; Zhan, W. C.; Liu, B. Mechanically Strong and Highly Conductive Graphene Aerogel and Its Use as Electrodes for Electrochemical Power Sources. *J. Mater. Chem.* **2011**, *21*, 6494−6497.
(21) Kim, K. H.; Oh, Y.; Islam, M. F. Graphene Coating Makes Carbon Nanotube Aerogels Superelastic and Resistant to Fatigue. *Nat. Nanotechnol.* **2012**, *7*, 562−566.
(22) Zou, J. H.; Liu, J. H.; Karakoti, A. S.; Kumar, A.; Joung, D.; Li, Q. A.; Khondaker, S. I.; Seal, S.; Zhai, L. Ultralight Multiwalled Carbon Nanotube Aerogel. *ACS Nano* **2010**, *4*, 7293−7302.
(23) Worsley, M. A.; Kucheyev, S. O.; Satcher, J. H.; Hamza, A. V.; Baumann, T. F. Mechanically Robust and Electrically Conductive Carbon Nanotube Foams. *Appl. Phys. Lett.* **2009**, *94*, 073115.
(24) Sun, H. Y.; Xu, Z.; Gao, C. Multifunctional, Ultra-Flyweight, Synergistically Assembled Carbon Aerogels. *Adv. Mater.* **2013**, *25*, 2554−2560.
(25) Zhao, Y.; Liu, J.; Hu, Y.; Cheng, H. H.; Hu, C. G.; Jiang, C. C.; Jiang, L.; Cao, A. Y.; Qu, L. T. Highly Compression-Tolerant Supercapacitor Based on Polypyrrole-Mediated Graphene Foam Electrodes. *Adv. Mater.* **2013**, *25*, 591−595.
(26) Nguyen, D. D.; Tai, N. H.; Lee, S. B.; Kuo, W. S. Superhydrophobic and Superoleophilic Properties of Graphene-Based Sponges Fabricated Using a Facile Dip Coating Method. *Energy Environ. Sci.* **2012**, *5*, 7908−7912.
(27) Tang, Z. H.; Shen, S. L.; Zhuang, J.; Wang, X. Noble-Metal-Promoted Three-Dimensional Macroassembly of Single-Layered Graphene Oxide. *Angew. Chem., Int. Ed.* **2010**, *49*, 4603−4607.
(28) Worsley, M. A.; Pauzauskie, P. J.; Olson, T. Y.; Biener, J.; Satcher, J. H.; Baumann, T. F. Synthesis of Graphene Aerogel with High Electrical Conductivity. *J. Am. Chem. Soc.* **2010**, *132*, 14067−14069.
(29) Worsley, M. A.; Olson, T. Y.; Lee, J. R. I.; Willey, T. M.; Nielsen, M. H.; Roberts, S. K.; Pauzauskie, P. J.; Biener, J.; Satcher, J. H.; Baumann, T. F. High Surface Area, sp(2)-Cross-Linked Three-Dimensional Graphene Monoliths. *J. Phys. Chem. Lett.* **2011**, *2*, 921−925.
(30) Chen, Z. P.; Ren, W. C.; Gao, L. B.; Liu, B. L.; Pei, S. F.; Cheng, H. M. Three-Dimensional Flexible and Conductive Interconnected Graphene Networks Grown by Chemical Vapour Deposition. *Nat. Mater.* **2011**, *10*, 424−428.
(31) Chen, Z. P.; Xu, C.; Ma, C. Q.; Ren, W. C.; Cheng, H. M. Lightweight and Flexible Graphene Foam Composites for High-Performance Electromagnetic Interference Shielding. *Adv. Mater.* **2013**, *25*, 1296−1300.
(32) Liu, Y.; Qian, W. Z.; Zhang, Q.; Cao, A.; Li, Z.; Zhou, W.; Ma, Y.; Wei, F. Hierarchical Agglomerates of Carbon Nanotubes as High-pressure Cushions. *Nano Lett.* **2008**, *8*, 1323−1327.
(33) Zhang, Q.; Zhao, M. Q.; Liu, Y.; Cao, A. Y.; Qian, W. Z.; Lu, Y. F.; Wei, F. Energy-Absorbing Hybrid Composites Based on Alternate Carbon-Nanotube and Inorganic Layers. *Adv. Mater.* **2009**, *21*, 2876−2880.
(34) Cai, D. K.; Neyer, A.; Kuckuk, R.; Heise, H. M. Raman, Mid-Infrared, Near-Infrared and Ultraviolet−Visible Spectroscopy of PDMS Silicone Rubber for Characterization of Polymer Optical Waveguide Materials. *J. Mol. Struct.* **2010**, *976*, 274−281.
(35) Stankovich, S.; Dikin, D. A.; Piner, R. D.; Kohlhaas, K. A.; Kleinhammes, A.; Jia, Y.; Wu, Y.; Nguyen, S. T.; Ruoff, R. S. Synthesis of Graphene-Based Nanosheets via Chemical Reduction of Exfoliated Graphite Oxide. *Carbon* **2007**, *45*, 1558−1565.
(36) Rao, A. M.; Eklund, P. C.; Bandow, S.; Thess, A.; Smalley, R. E. Evidence for Charge Transfer in Doped Carbon Nanotube Bundles from Raman Scattering. *Nature* **1997**, *388*, 257−259.
(37) Kitaura, R.; Imazu, N.; Kobayashi, K.; Shinohara, H. Fabrication of Metal Nanowires in Carbon Nanotubes via Versatile Nano-Template Reaction. *Nano Lett.* **2008**, *8*, 693−699.
(38) Zhou, J. S.; Song, H. H.; Ma, L. L.; Chen, X. H. Magnetite/Graphene Nanosheet Composites: Interfacial Interaction and Its Impact on the Durable High-Rate Performance in Lithium-Ion Batteries. *RSC Adv* **2011**, *1*, 782−791.
(39) Zhou, G. M.; Wang, D. W.; Yin, L. C.; Li, N.; Li, F.; Cheng, H. M. Oxygen Bridges between NiO Nanosheets and Graphene for Improvement of Lithium Storage. *ACS Nano* **2012**, *6*, 3214−3223.
(40) Schaedler, T. A.; Jacobsen, A. J.; Torrents, A.; Sorensen, A. E.; Lian, J.; Greer, J. R.; Valdevit, L.; Carter, W. B. Ultralight Metallic Microlattices. *Science* **2011**, *334*, 962−965.
(41) Gui, X. C.; Cao, A. Y.; Wei, J. Q.; Li, H. B.; Jia, Y.; Li, Z.; Fan, L. L.; Wang, K. L.; Zhu, H. W.; Wu, D. H. Soft, Highly Conductive Nanotube Sponges and Composites with Controlled Compressibility. *ACS Nano* **2010**, *4*, 2320−2326.
(42) Yong, J. L.; Chen, F.; Yang, Q.; Zhang, D. S.; Bian, H.; Du, G. Q.; Si, J. H.; Meng, X. W.; Hou, X. Controllable Adhesive Superhydrophobic Surfaces Based on PDMS Microwell Arrays. *Langmuir* **2013**, *29*, 3274−3279.
(43) Tian, S. B.; Li, L.; Sun, W. N.; Xia, X. X.; Han, D.; Li, J. J.; Gu, C. Z. Robust Adhesion of Flower-Like Few-Layer Graphene Nanoclusters. *Sci. Rep.* **2012**, *2*, 511.
(44) Feng, L.; Zhang, Y. A.; Xi, J. M.; Zhu, Y.; Wang, N.; Xia, F.; Jiang, L. Petal Effect: A Superhydrophobic State with High Adhesive Force. *Langmuir* **2008**, *24*, 4114−4119.
(45) Xi, J. M.; Jiang, L. Biomimic Superhydrophobic Surface with High Adhesive Forces. *Ind. Eng. Chem. Res.* **2008**, *47*, 6354−6357.
(46) Liu, M. J.; Zheng, Y. M.; Zhai, J.; Jiang, L. Bioinspired Super-Antiwetting Interfaces with Special Liquid−Solid Adhesion. *Acc. Chem. Res.* **2010**, *43*, 368−377.
(47) Darmanin, T.; Givenchy, E. T.; Amigoni, S.; Guittard, F. Superhydrophobic Surfaces by Electrochemical Processes. *Adv. Mater.* **2013**, *25*, 1378−1394.
(48) Winkleman, A.; Gotesman, G.; Yoffe, A.; Naaman, R. Immobilizing a Drop of Water: Fabricating Highly Hydrophobic Surfaces That Pin Water Droplets. *Nano Lett.* **2008**, *8*, 1241−1245.
(49) Laird, E. D.; Wang, W. D.; Cheng, S.; Li, B.; Presser, V.; Dyatkin, B.; Gogotsi, Y.; Li, C. Y. Polymer Single Crystal-Decorated

Superhydrophobic Buckypaper with Controlled Wetting and Conductivity. *ACS Nano* **2012**, *6*, 1204−1213.